BEAM DIAGNOSTICS WITH SYNCHROTRON RADIATION IN LIGHT SOURCES

S. Takano*
Japan Synchrotron Radiation Research Institute, SPring-8, Sayo, Hyogo, 679-5198, Japan

Abstract

Topics of beam instrumentation on light sources based on synchrotron radiation (SR) for transverse beam profiling, longitudinal bunch profiling, and bunch purity measurement will be given. Developments of beam diagnostics based on observation of x-rays from a dedicated insertion device (ID) will also be presented.

INTRODUCTION

SR is the versatile tool for non-destructive characterizations of the electron/positron beam in the storage rings. In this paper, topics of beam instrumentation on light sources based on SR will be presented. A brief overview of the beam profiling instrumentation will be given as well as recent developments to improve the spatial resolution. A number of novel methods will be given for longitudinal bunch profiling and bunch purity measurement. Finally, examples of beam diagnostics based on observation of x-rays from a dedicated ID will be presented.

TRANSVERS BEAM PROFILING

The non-destructive transverse beam profiling based on SR is the key instrumentation for emittance diagnostics of the source electron/positron beam in the light sources. The beam emittance is calculated from the measured beam size with knowledge of the machine parameters such as the beta and dispersion functions and the relative energy spread by the formula,

$$\varepsilon_i = \frac{\sigma_i^2 - (\sigma_E/E)^2 \eta_i^2}{\beta_i} \quad i = x,y \quad .$$

Light sources are now competing to achieve lower emittance and emittance coupling ratio to increase the brilliance of the SR [1]. The minimum vertical emittance ε_y achieved is now approaching to 1 pm rad [2]. At the source point of the SR based beam profiling in a dipole magnet the vertical beta function β_y is a few tens of meters, and the corresponding beam size σ_y is several microns or even less. The spatial resolution better than a few microns is now demanded for transverse beam profiling on the most performing light sources. An excellent and comprehensive review of the SR based diagnostics for transverse profile measurements has been given recently [3]. A brief overview as well as recent developments shall be given here. The simple imaging in the visible/UV band has no longer enough spatial resolution to resolve the vertical dimension of the beam due to diffraction effects, and a variety of different methods have been elaborated.

A list of beam profiling instrumentation in light sources is given in table 1. The operating wavelength regions of the beam profiling instruments can be divided in two bands, the X-ray band and the visible/UV band. The most straightforward way to overcome the resolution limit imposed by diffraction is to image the beam at the shorter wavelength in the X-ray region. X-ray pinhole cameras are now widely used as for example at ESRF [4], BESSY II [5], APS [6], ALS [7], SLS [8], SOLEIL [9], Diamond [2], ASP [10], CLS [11], SSRF [12] SPEAR3 [13] and PETRA III [14], and are planned at ALBA [15] and NSLS-II [16]. A schematic setup of an X-ray pinhole camera is shown in Fig. 1. The simplistic estimation of

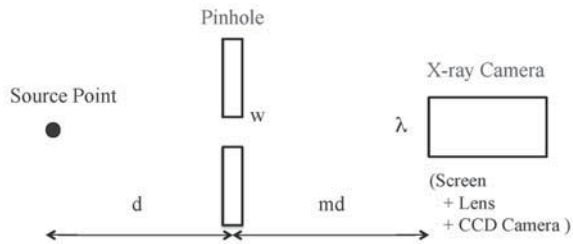

Figure 1: Schematic setup of an X-ray pinhole camera.

the spatial resolution of an X-ray pinhole (rms width of the point-spread function at the source point) is given by

$$S_{Pinhole}^{\ 2} = S_{Diffraction}^{\ 2} + S_{Aperture}^{\ 2}$$

where

$$S_{Diffraction} = \frac{0.36\lambda d}{w}, \qquad S_{Aperture} = \frac{w(1+1/m)}{\sqrt{12}}$$

are contributions of diffraction and finite aperture of the pinhole, respectively. Given the geometry of the system (d, and md) and the observing wavelength λ, the optimum resolution is

$$S_{Pinhole\_opt} = 0.46\sqrt{\lambda d\left(1+\frac{1}{m}\right)}$$

for optimized pinhole size of

$$w_{opt} = 1.12\sqrt{\frac{\lambda d}{1+1/m}} \quad .$$

While precise quantitative determination of the spatial resolution of the pinhole imaging demands calculation of the point-spread function based on wave optics taking account of the finite bandwidth of the SR detected, the simplistic formula above shows that the better spatial resolution is obtained for shorter source to pinhole distance d, larger magnification m, and shorter observing wavelength λ. The state-of-the-art X-ray pinhole cameras as for example at SOLEIL [9], Diamond [2], and

*takano@spring8.or.jp

Table 1: List of Beam Profiling Instrumentation in Light Sources

σ_y : vertical beam size, measured minimum (resolution subtracted) or targeted
$\Delta\sigma_y$: overall spatial resolution of the instrument at the source point

	Energy (GeV)	ε_x (nm rad)	ε_y (pm rad)	σ_y (μm)	$\Delta\sigma_y$ (μm)	X-ray	Visible/UV	References
SPring-8	8	3.4	7.2	14.1	4.1 -	Zone Plate	 2-dim. Inter.	[20] [30]
PF	2.5	35.5	244	42.2	-		1-dim. Inter.	[25]
UVSOR-II	0.75	27.4	<274	<80	-		1-dim. Inter.	[26]
PLS	2.5	12		43		K-B mirror		[19]
TLS	1.5	21.5	55.5	30	-		1-dim. Inter.	[27]
SSRF	3.5	3.9	47	34	10 -	Pinhole	 1-dim. Inter.	[12] [28]
ASP	3	10.4	4.5	~20	~65	Pinhole		[10]
ESRF	6	3.7	7	16	3.5 -	Pinhole In air X-ray		[17] [22]
SLS	2.4	5.6	3.2	6.4	- 9	 Pinhole	π-polarization	[32] [8]
BESSY II	1.7	5.2	<100	40	3 11	BF lens Pinhole		[5] [5]
MAX II	1.5	9		30	-		π-polarization	[31]
ANKA	2.5	50		34	-	In air X-ray		[23]
SOLEIL	2.75	3.7	3.7	< 8.4	~5	Pinhole		[9]
Diamond	3	2.7	1.7	5.9	3.4	Pinhole		[2]
ALBA	3	4.3	43	32	~15	Pinhole		[15]
PETRA III	6	1	10	18.5	1~2 16	CR lens Pinhole		[14] [14]
APS	7	2.5	40	-	~12	Pinhole		[6]
ALS	1.9	6.3	~5	~10	- 33	K-B mirror Pinhole		[18] [7]
SPEAR3	3	10	<10	~20	>10 -	Pinhole	 1-dim. Inter.	[13] [29]
CLS	2.9	18	~30	~30	~11	Pinhole		[11]
NSLS-II	3	0.5 - 2	8	12	2 9	CR lens Pinhole		[21] [16]

ESRF [17] have been elaborately designed and have achieved the system resolution better than 5 μm.

The X-ray focusing optics has potentials to attain superior spatial resolution with the advantage of larger aperture than a pinhole. The X-ray imaging systems based on the Kirkpatric-Baez mirror are used at ALS [18] and PLS [19], and the Bragg-Fresnel multi-layer optics is used at BESSY II [5]. The X-ray Beam Imager at SPring-8 uses a single Fresnel zone plate (FZP) [20]. The FZP is made of Ta 2.0 μm thick and has the effective diameter of 1.4 mm. The electron beam is imaged on to an X-ray zooming tube with SR monochromatized at 8 keV by a Si (111) double crystal monochromator. While the theoretical resolution of the FZP is 1.5 μm, the system resolution is 4.1 μm dominated by the contribution of the X-ray zooming tube. The X-ray imaging system based on the compound refractive lens (CRL) optics is being commissioned at PETRA III [14]. The CRL system consists of 31 individual lenses made of Be and has a geometrical aperture of 0.9 mm. A single crystal Si (311) monochromator in Laue geometry is used to obtain monochromatic SR at 20 keV. The theoretical resolution of the CRL optics is 0.2 μm, and the total system resolution is limited by the resolution of the X-ray detector system. A high resolution X-ray CCD system is in preparation to improve the resolution of 6 μm obtained by the current detector system down to the level of 1-2 μm. Usage of CRL optics is being considered at NSLS-II [21].

The in-air-X-ray (IAX) monitors at ESRF [22] and ANKA [23] measures in the air just behind the dipole crotch absorbers the vertical dimension of the penetrating hard X-rays of the SR (>150keV at ESRF and >70 keV at ANKA, respectively). With knowledge of the distance to

the source, the vertical beta function and the natural photon beam divergence, the vertical beam emittance is obtained from the measured height of the X-rays.

In the visible light region to overcome the limit by diffraction effects, the application of the interferometry was noted [24]. The so-called SR interferometer uses a double slit to obtain one-dimensional interference pattern along the horizontal or vertical axis. A schematic setup of a SR interferometer is shown in Fig. 2. The intensity of

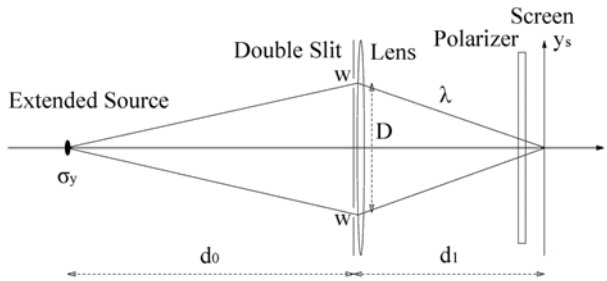

Figure 2: Schematic setup of a SR interferometer.

interference pattern on the screen is given by

$$I = I_0\left\{\mathrm{sinc}\left(\pi\frac{y_s}{y_0}\right)\right\}^2\left[1+V\cos\left(2\pi\frac{D}{w}\cdot\frac{y_s}{y_0}\right)\right], \qquad y_0 = \frac{d_1\lambda}{w}$$

Extended dimension of the source smears out the interference fringe, and the source size σ_y is related to the visibility of the fringe V by the formula,

$$V = \frac{I_{\max}-I_{\min}}{I_{\max}+I_{\min}} = \exp\left(-2\frac{\pi^2 D^2\sigma_y^{\,2}}{\lambda^2 d_0^{\,2}}\right) \quad .$$

The SR interferometer is widely used as for example at PF [25], UVSOR-II [26], TLS [27], SSRF [28] and SPERA-III [29].

At SPring-8 a sophisticated two-dimensional SR interferometer has been developed [30]. Instead of a standard double slit, it uses a diffracting mask with four apertures distributed at the corners of a rectangle. The transverse distribution of the beam is modelled by an elliptical Gaussian distribution. Its three parameters, the beam sizes along the major and the minor axes, and the tilting angle of the major axis, are determined by fitting to the observed two-dimensional interference pattern a model function, which is obtained by convoluting the point-spread function with a Gaussian distribution. More simply by projecting the two-dimensional interference pattern on each axis, horizontal or vertical, one-dimensional interference pattern can be obtained, and the projected source beam size can be calculated by the visibility formula as in the case of the standard SR interferometer.

At MAX II a different approach has been implemented to improve the resolution of the imaging in the visible region [31]. By selecting the π-polarization component, double-peaked intensity distribution in the vertical with minimum at the center is observed on the detector plane. The increased source dimension in the vertical fills out the central dip. By comparing the measured peak-to-valley ratio with the theoretical prediction based on a near-field SR calculation, the vertical beam size can be deduced. At SLS the same method has been applied at 364 nm in the UV region, and small beam size of 6.4 μm has been successfully measured [32].

LONGITUDNAL BUNCH LENGTH MEASUREMENTS

Two topics of recent developments of bunch length measurements are briefly described. One is based on the statistical analysis of the intensity fluctuations and the other on the cross-correlation of the SR pulse and the external laser pulse.

It has been shown theoretically that by measuring the fluctuation of the intensity of the SR in a part of the spectrum where the emission is incoherent, the bunch length can be measured [33]. The proof-of-principle experiment was conducted successfully at the ATF at BNL [34]. The single-shot spectrum of spontaneous emission from an undulator was measured for the first time with the resolution and sensitivity required to study its fluctuational characteristics. The length of a 1-5 ps long bunch was extracted from fluctuations and agreement was obtained between experiment and theory, and with an independent bunch length measurement technique. Recently a simpler scheme based on the principle has been developed at ALS [35]. The radiation intensity from a dipole magnet emitted during a single beam passage is measured within a fixed bandwidth Δω by using a narrow band-pass filter (centered at 632.8 nm with a bandwidth of 1 nm FWHM) and an avalanche photodiode (APD). The bunch length is determined by the statistical analysis of the turn by turn intensity fluctuation. The result is in good agreement with streak-camera data and the capability of the method for an absolute bunch length measurement has been successfully demonstrated.

The cross-correlation between the SR beam and the mode-locked laser beam has been first applied for longitudinal bunch profile measurement successfully at ALS [36]. The principle of the measurement is to interact a short-pulse laser with the longer SR pulse in a non-linear crystal (BBO) to generate a signal at the up-converted frequency of the sum of the laser and the SR frequencies. The monochromatic SR can be obtained by a narrow band-pass filter. When the laser and SR pulse do overlap, there is signal proportional to the SR intensity at time where the SR pulse and laser pulse are coincident. In order to measure the SR pulse profile, the laser pulse is scanned with respect to the SR pulse in time. The overlap time is as long as the laser pulse, and the time resolution better than 1 ps is expected by employing the laser with short pulse. Recently at SPEAR3, the experiment of this technique employing a 50 fs mode-locked laser is in progress in order to quantify the bunch length of the order of ~1ps obtained by operating the ring in the quasi-isochronous (low-alpha) mode [37].

BUNCH PURITY MEASUREMENTS

For time resolved user experiments, light sources are operated with bunch filling patterns with one or more

isolated bunches. The bunch purity is defined as the relative intensity ratio of the unwanted satellite bunches with respect to the main bunches. The time-correlated single photon counting (TCSPC) is the method widely used to measure the bunch purity [38]. In the TCSPC a fast photon detector capable of detecting a single photon is used as for example a MCP-PMT for the visible photons, and an APD for the X-ray photons. The time difference of the single photon signal with respect to the clock pulse synchronized to the rf signal is processed by the time-to-digital converter, and the histogram of the photon arrival time which represents the bunch filling pattern is accumulated. While the TCSPC has a dynamic range of 10^{-6} to 10^{-7}, the conventional time-to-digital conversion based on a time-to-amplitude convertor (TAC) and a multi-channel analyzer (MCA) was subject to dead time. At APS a fast time-to-digital convertor with a maximum counting rate of 50 MHz has been implemented based on a field programmable array (FPGA) [39]. At BESSY II [40], Diamond [41], ASP [42], TLS [43], and SLS, a newly developed commercial stand-alone time-to-digital conversion unit, the PicoHarp 300 (PicoQuant) [44] is used, which has a maximum counting rate of 10 MHz.

At SPring-8 fast light shutter systems have been developed for the TCSPC system of the visible photons [45]. The light shutter consists of a pair of crossed polarizers and a Pockels in between. By applying a high voltage (HV) pulse to the Pockels cell the polarization of the light is rotated and the light shutter is opened. The time response of the light shutter is determined by that of the HV pulse. The rise/fall time, the width and the repetition frequency of the HV pulse are < 2 ns (bunch spacing), 2 ns, and 209 kHz (the revolution frequency of SPring-8), respectively. To improve the extinction ratio, two light shutter systems are arranged in tandem. By gating the copious photons from the main bunches, the dynamic range has been improved and satellite bunches with relative intensity of 10^{-10} to the main bunches can be detected.

DIAGNOSTICS BEASED ON A DEDICATED ID

By observing the imprints on the spectral, spatial, and temporal characteristics of SR of an ID such as an undulator, both transversal and longitudinal properties of the electron beam can be characterized. At ESRF an emittance monitor based on the X-ray beam from a dedicated undulator was developed [46]. The white beam was monochromatized by a Si crystal at 28 keV, which corresponded to the seventh undulator harmonic, and was projected onto a screen at a known distance from the source. The emittance was deduced form the measured photon beam size with knowledge of lattice beta functions and the natural photon beam divergence. The minimum detectable emittance of this technique was about 100 pm rad, which was limited by the natural photon beam divergence. A refinement of this setup is now being implemented at the beamline ID30 [47].

At the APS diagnostic undulator line, simultaneous measurement of the divergence and the size of the electron beam was demonstrated [48]. A 300-μm-thick Si crystal monochromator was used to measure the divergence, and the X-rays transmitted through the crystal were simultaneously used by a pinhole camera to measure the beam size. Multiplying the effective beam divergence and size measured, the horizontal beam emittance was successfully obtained independent of the knowledge of lattice functions.

Simultaneous measurement of the emittance and the energy spread of the electron beam by observing the divergence of higher harmonics of the dedicated ID has been recently studied at the SPring-8 diagnostics beamline II [49]. In the case of the radiation of a single electron, the higher harmonics have much narrower spectral bandwidth and smaller angular divergence than those of the fundamentals, which are the advantages for the emittance and energy spread diagnostics. The vertical divergence of photon beam of higher harmonics of the ID is sensitive to the energy spread of the electron beam because of the small vertical emittance of SPring-8, while the horizontal divergence is dominated by the horizontal emittance. The major advantage of the spatial measurement compared with the spectral measurement, which demands scanning of the monochromator, is the promptness. A fast turn-by-turn system for simultaneous measurement of the emittance and the energy spread of the beam is now under development which is expected to be useful for curing unexpected instabilities of the stored beam and for tuning the injection of the high quality beam to be delivered from the C-band XFEL driver.

SUMMARY

Topics of beam instrumentation on light sources based on SR are presented. A brief overview of the transverse beam profiling instrumentation is given. X-ray pinhole cameras and visible SR interferometers are widely used. Developments of imaging systems based on the X-ray focusing optics are pursued to improve the spatial resolution. Regarding the longitudinal diagnostics, bunch length measurements based on the statistical analysis of the intensity fluctuations and on the cross-correlation of the SR and the external laser pulse are described as well as the bunch purity measurement by using a fast light shutter. Finally, examples of beam diagnostics based on observation of x-rays from a dedicated ID are presented.

ACKNOWLEDEGMENTS

I would like to thank many specialists and experts on beam diagnostics and instrumentation from various light sources for providing me with valuable information of their elaborate instruments and for stimulating comments and discussions.

REFERENCES

[1] R. Bartolini, Proc. EPAC'08 (2008) p.993.
[2] C. Thomas et al., Phys. Rev. ST Accel. Beams 13 (2010) 022805.
[3] G. Kube, Proc. DIPAC'07 (2007) p.6.
[4] P. Elleaume et al., J. Synch. Rad. 2 (1995) p.209.
[5] K. Holldack et al., Nucl. Instr. and Meth. A467 (2001) p.235.
[6] M. Borland et al., Proc. EPAC'98 (1998) p.1556.
[7] F. Sannibale et al., Proc. EPAC'04 (2004) p. 2783.
[8] Å. Andersson et al., Proc. DIPAC'07 (2007) p.129.
[9] M.-A. Tordeux et al., Proc. DIPAC'07 (2007) p.180.
[10] M.J. Boland et al., Proc. EPAC'08 (2008) p. 1059.
[11] J.C. Bergstrom, J. M. Vogt, Nucl. Instr. and Meth. A587 (2008) p.441.
[12] Y.B. Leng et al., Proc. DIPAC'09(2009)p.29.
[13] J. Corbett et al., Proc. EPAC'06 (2006) p. 1259.
[14] G. Kube et al., Proc. IPAC'10, MOPD089.
[15] U. Iriso, F. P´erez, Proc. EPAC'06 (2006) p.3410.
[16] I. Pinayev et al., Proc. PAC'09, TH5RFP015.
[17] B.K. Scheidt, private communications.
[18] T.R. Renner et al., Rev. Sci. Instr. 67 (1996) p.3368.
[19] J.Y. Huang et al., Proc. PAC'99 (1999) p.2131.
[20] S. Takano, et al., Nucl. Instr. and Meth. A556 (2006) p.357.
[21] P. Ilinski, private communications.
[22] B.K. Scheidt, Proc. DIPAC'07 (2007) p.72.
[23] A.-S. M¨uller et al., Proc. EPAC'06 (2006) p.1073.
[24] T. Mitsuhashi, Proc. PAC'07 (1997) p.766.
[25] Photon Factory Activity Report 2007 Part A (2007) p.118.
[26] M. Katoh, private communications.
[27] T.C. Tseng et al., Proc. PAC'05 (2005) p.3465.
[28] K.R. Ye et al., Proc. DIPAC'09(2009) p.381.
[29] J. Corbett et al., Proc. PAC'09, TH6REP033.
[30] M. Masaki, S. Takano, J. Synch. Rad. 10 (2003) p.295.
[31] M. Sjöström et al., EPAC'06 (2006) p.1193.
[32] Å. Andersson et al., Nucl. Instr. and Meth. A591 (2008) p.437.
[33] M.S. Zolotorev and G.V. Stupakov, SLAC-PUB-7132 (1996).
[34] P. Catravas et al., Phys. Rev. Lett. 82 (1999) p.5261.
[35] F. Sannibale et al., Phys. Rev. ST Accel. Beams 12 (2009) 032801.
[36] M. Zolotorev et. al., Proc. PAC'03 (2003) p.2530.
[37] J. Corbett, Proc. IPAC'10, WEOCMH03.
[38] D.V. O'Connor, D. Phillips, Time-correlated Single Photon Counting, Academic Press, London, 1984
[39] W.E. Norum, B. Yang, Proc. PAC'07 (2007) p.4386.
[40] K. Holldack et al., Proc. SPIE 6771 (2007) .
[41] C.A. Thomas et al., Nucl. Instr. and Meth. A566 (2006) p.762.
[42] M.J. Boland et al., Proc. PAC'07 (2007) p.3856.
[43] C.Y. Wu et al, Proc. EPAC'08 (2008) p.1137.
[44] http://www.picoquant.de/index.php
[45] K. Tamura, T. Aoki, Proc. 1st Annual Meeting of Particle Accelerator Society of Japan 2004 (2004) p.581.; http://www.pasj.jp/web_publish/pasj1_lam29/WebPublish/5P50.pdf
[46] E. Tarazona, P. Elleaume, Rev. Sci. Instrum. 66 (1995) p.1974.
[47] F. Ewald, Proc. DIAPC'09 (2009) p.182.
[48] B.X. Yang, A.H. Lumokin, Proc. PAC'99 (1999) p.2161.
[49] M. Masaki et al., Proc. SRI'09, AIP Conf. Proc. 1234 (2010) p.554.